ENHANCING CONTRAST OF IMAGES TO IMPROVE GEOMETRIC ACCURACY OF A UAV PHOTOGRAMMETRY PROJECT

Soroush Motayyeb [1], Seyed Arya Fakhri [2], Masood Varshosaz [3], Saied Pirasteh [4] *

[1] Dept. of Photogrammetry and Remote Sensing, School of Surveying and Geospatial Engineering, University College of Engineering, University of Tehran, Tehran, Iran - soroush.motayyeb@ut.ac.ir

[2] Dept. of Geomatic Engineering, Faculty of Civil Engineering and Transportation, University of Isfahan, Isfahan, Iran - aryafakhri@trn.ui.ac.ir

[3] Dept. of Engineering, K. N. Toosi University of Technology, Tehran, Iran - varshosazm@kntu.ac.ir

[4] Dept. of Surveying and Geoinformatics, Faculty of Geosciences and Environmental Engineering (FGEE), Southwest Jiaotong University, Chengdu 611756, S.P., China - sapirasteh@swjtu.edu.cn

KEY WORDS: UAV photogrammetry, image contrast enhancement, image matching, point cloud.

ABSTRACT:

In recent years, Unmanned Aerial Vehicles (UAVs) have become popular tools in mapping applications. In such applications, the image motion, bad lighting effects, and poor texture all directly affect the quality of the derived tie points, which in turn imposes constraints on image extraction and may lead to a low accuracy point cloud. This paper proposes a contrast enhancement technique to improve the accuracy of a photogrammetric model created using UAV images. The luminance component (Y) in the YIQ color space is normalized using the sigmoid function, and the low contrast images are enhanced using the Contrast-Limited Adaptive Histogram Equalization (CLAHE) on the luminosity component. To evaluate the proposed method, three-dimensional models were created using images acquired by the Phantom 4 Pro UAV in three distinct places and at altitudes of 20, 40, 60, 80, and 90 meters. The results showed that enhancing the contrast of images increased the number of tie points and reduced reprojection error by approximately 10%. It also improved the resolution of the digital elevation model by approximately 2cm/pixel while greatly improving the texture and quality with respect to that developed using the original images.

1. INTRODUCTION

Today, given the relevance of three-dimensional models in a wide variety of computer vision applications, a large number of academics are studying the issues of reconstructing three-dimensional models from two-dimensional images (Alasal et al., 2018). Without a doubt, approaches for three-dimensional reconstructing using images have advanced beyond the shadow of laser scanning (Luhmann et al., 2020). Thus, by combining automated computer vision algorithms with trustworthy and precise photogrammetric methods, successful solutions for automatic and accurate three-dimensional reconstruction of picture data sets are created (Demetrescu et al., 2020; Pepe and Costantino, 2020; Qin and Gruen, 2021). Meanwhile, the rapid growth of unmanned aerial vehicles (UAVs) in recent years and their ability to provide high resolution and accuracy information has improved UAV photogrammetry projects. Moreover, their versatility in data acquisition, as well as the combination of different sensors and the use of three-dimensional model production algorithms such as Structure from Motion (SfM) and Multi View-Stereo (MVS) (Moons et al., 2009; Skarlatos and Kiparissi, 2012) has been used in a variety of applications such as surveying and forestry (Chang et al., 2020; Fakhri and Latifi, 2021), archaeology (Jacq et al., 2021), civil engineering (Lv et al., 2021), and documentation (Godinho et al., 2020). These advancements have transformed drone systems into standard platforms for collecting three-dimensional data (Jarzabek-Rychard and Karpina, 2016; Yao et al., 2019).

To create a three-dimensional model of images, the scene's objects can be modelled as “active” or “passive” (Alasal et al., 2018). Three-dimensional modelling was accomplished by using the active technique by modifying illumination conditions, controlling camera angles, and also utilizing the camera’s predetermined calibration parameters (Fakhri and Fakhri, 2019). However, in passive techniques, the quality of the images may be compromised due to the lack of control over lighting conditions and the utilization of the solar energy source (Arroyo-Mora et al., 2021; Revuelto et al., 2021). As a result, optimizing image acquisition quality prior to performing three-dimensional reconstruction operations becomes a critical requirement in autonomous three-dimensional reconstruction approaches.

In general, extensive research has been conducted to improve the 3D model's quality. The research conducted in this field can be classified into two broad categories. In the first view, pre-processing is used on the images to remove any negative conditions that may affect the matching results (Ballabeni et al., 2015; Bellavia et al., 2015; Gaiani et al., 2016; Maini and Aggarwal, 2010; Verhoeven et al., 2015). Researchers typically undertake pre-processing on the photos when reviewing the aforementioned methods, such as applying initial adjustments. Or, by employing more complex filters, the quality of the 3D model created by automated image-based methods can be improved. In comparison to the original images, these methods significantly improve the correlation quality and the external orientation accuracy of images and point clouds. However, this approach lacks control over the distribution and quality of selected tie points within the image, and it is incapable of extracting points from a large number of repeats, causing the other significant aspects to become uncontrollable.

In the second view, picture matching efficiency has been enhanced in the feature selection stage by identifying image characteristics with a stricter threshold. By examining the

* Corresponding author

methods available in this approach (Dymczyk et al., 2016; Hartmann et al., 2014; Wu, 2013), classifications can be made based on the identification of image features using a more stringent threshold, which increases computational speed when fewer features but higher contrast are used. These methods have several limitations, including the elimination of a large number of suitable points as the threshold is increased, the uncertainty of features with lower resolution in the location, the requirement for high-quality training data to teach classification algorithms, and a disregard for multiplicity. Highlighted features on the image, and so forth. Thus, by comparing the research conducted in the two approaches above, it can be concluded that in the methods used to improve image matching conditions, additional corrections such as image contrast enhancement, noise removal, image content enhancement, and color conversion to Grayscale are discussed, all of which can contribute significantly to improving image matching conditions by creating color balance in images and enhancing coherence.

As a result, this study investigates the effect of contrast-enhanced images acquired by UAV platforms in low-light conditions prior to producing a three-dimensional model; thus, the primary objective of this research is to determine the effect of contrast-enhanced images on the preparation of a three-dimensional model from the perspective of image matching and point cloud density, as well as the effect on triangulation accuracy, check point accuracy, digital elevation model accuracy and orthophoto mosaic quality.

Section 2 details the suggested algorithm's method and flowchart. Section 3 presents the results and evaluations of the proposed algorithm's implementation, followed by a conclusion.

2. PROPOSED METHOD

Two tasks (Figure 1.) are accomplished in this paper:

a) The proposed algorithm for image contrast enhancement and its comparison to existing approaches.
b) Construction and evaluation of a three-dimensional model.

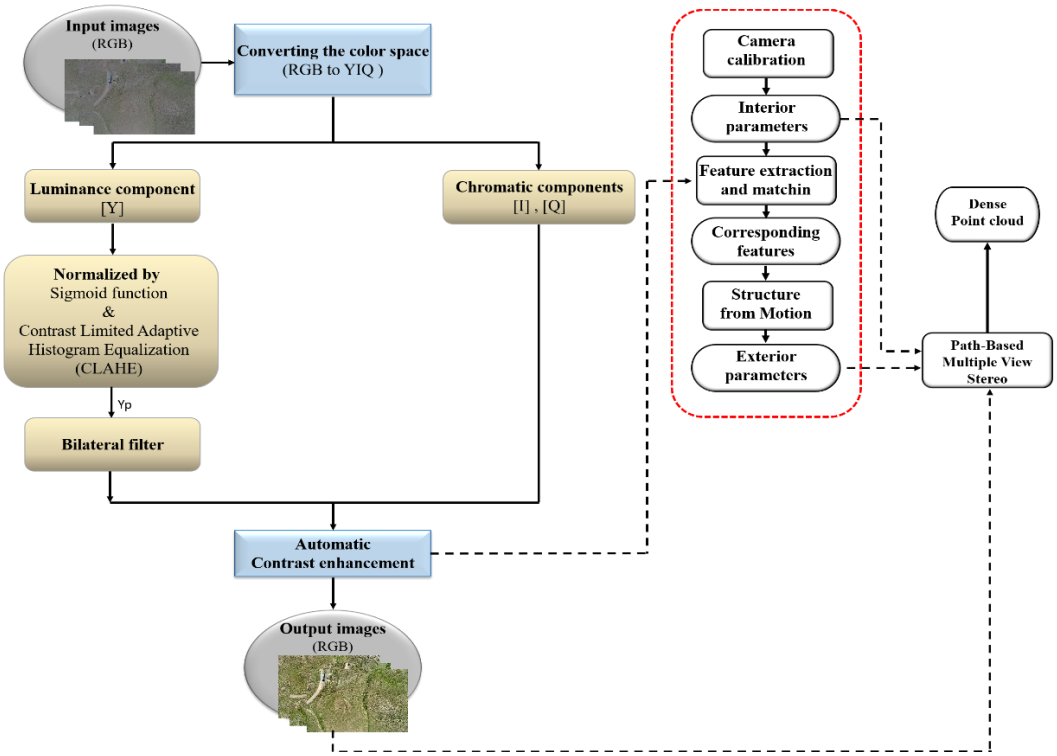

Figure 1. The flowchart of the method.

According to the flowchart above, in order to study the influence of image contrast enhancement on the three-dimensional model generated using UAV photogrammetry, it is necessary to first enhance the low-contrast images in the pre-processing stage using the proposed technique. The three-dimensional point cloud and other photogrammetric products such as the digital elevation model and orthophoto mosaic are then generated using contrast-enhanced images. Finally, the relevant assessments will be reviewed in order to assess the suggested algorithm's effectiveness and the three-dimensional model generated using various criteria.

2.1 The proposed algorithm for image contrast enhancement

The proposed method for enhancing the contrast of images collected by UAV photogrammetry is based on research (Lal et al., 2015). To enhance the contrast of the images in the preceding research (Lal et al., 2015), the RGB color space was transformed to YIQ (Equation 1), a technique that requires two processing stages. The luminance component (Y) is normalized in the YIQ color space using the sigmoid function (Equation 2), and the resulting component (YP) is applied using the adaptive histogram equalization (AHE) method (Pizer et al., 1987). The images are then subjected to the auto-contrast enhancement method in the following stage.

To develop the study's main idea (Lal et al., 2015), after normalizing the luminance component (Y) with the sigmoid function and in accordance with research results (Lestari and Luthfi, 2019), which indicate that the Contrast-Limited Adaptive Histogram Equalization (CLAHE) (Zuiderveld, 1994) approach outperforms AHE. CLAHE is applied on the luminance

component (Y). The images are then enhanced using the auto-contrast enhancement approach (Lal et al., 2015). On the images, a Bilateral filter (Tomasi and Manduchi, 1998) was employed to remove noise produced by the CLAHE approach. The Bilateral filter is a nonlinear filter that smooths the image's edges and reduces noise; it preserves the image's main edges and results in a smooth image with edges and noise reduction (Paris et al., 2009; Tomasi and Manduchi, 1998).
Equation 1: (Recommendation, 2005; Standard, 2003) and Equation 2: (Hertz et al., 2018).

$$\begin{aligned} Y &= 0.299R + 0.587G + 0.114B \\ I &= 0.596R - 0.275G - 0.321B \\ Q &= 0.212R - 0.523G - 0.311B \end{aligned} \quad (1)$$

$$S_n(x,y) = \frac{1}{\left(1 + \sqrt{\frac{(1 - I_n(x,y))}{I_n(x,y)}}\right)} \quad (2)$$

Where I_n denotes the component of luminance (Y).

2.2 Evaluation of the proposed algorithm for contrast enhancement

To evaluate and compare the proposed contrast-enhancement algorithm's performance, several commonly used algorithms such as HE (Pizer et al., 1987), CLAHE, and AMCE (Lal et al., 2015) are analyzed using a variety of evaluation criteria. These are the following criteria:
Equation 3: Shannon entropy (Shannon, 1948).

$$E(I) = -\sum_{i=0}^{L-1} p_i \log_2(p_i) \quad (3)$$

Where I is the original image (reduced), pi denotes the probability that the value of i occurs in image I, in other terms, the variable p is computed from the gray values of the image histogram (for example, Pi comprises the values of the i level), L = 2q denotes the number of various grayscale values, as well as q bits per pixel.
Equation 4: Standard deviation (SD) (Román et al., 2017).

$$SD(I) = \sqrt{\sum_{k=0}^{L-1} (k - A(I))^2 \times p(k)} \quad (4)$$

Where k denotes the numerical value of the pixel in the original image (reduced), I, L - 1 denotes the maximum grayscale, A (I) denotes the average grayscale intensity of the image, and p (k) denotes the probability of the value of k occurring.
Equations 5 and 5-1: Peak signal-to-noise ratio (PSNR) and Mean Squared Error (MSE) (Hore and Ziou, 2010).

$$PSNR\ (I, I_E) = 10 \times log_{10}\ \frac{(L-1)^2}{MSE\ (I, I_E)} \quad (5)$$

$$MSE\ (I, I_E) = \frac{1}{M \times N} \sum_{u=0}^{M-N-1} \sum_{v=0}^{-1} (I(u,v) - I_{EN}(u,v))^2 \quad (5\text{-}1)$$

The peak signal-to-noise ratio is defined as M × N according to the size of the original image (reduced) and enhanced image.
Equation 6: Absolute Mean Brightness Error (AMBE) (Phanthuna, 2015).

$$AMBE\ (I, I_E) = |A(I) - A(I_E)| \quad (6)$$

Where I and I_E represent the original image (reduced) and enhanced, respectively, A (I) and A (I_E) represent the mean brightness of the aforementioned images.
Equations 7 and 7-1: The linear blur index (Kaufmann, 1975).

$$\gamma(I) = \frac{2}{M \times N} \sum_{v=1}^{M} \sum_{v=1}^{N} min\{p_{uv}, (1 - p_{vv})\} \quad (7)$$

$$p_{uv} = sin\left[\frac{\pi}{2} \times \left(1 - \frac{I(u,v)}{L-1}\right)\right] \quad (7\text{-}1)$$

Where M × N are the dimensions of the original image (reduced), I (u, v) are the grayscale values of the image pixels (u, v) and L - 1 is the maximum grayscale value of the image I.
Equation 8: Colorfulness (CM) (Susstrunk and Winkler, 2003).

$$CM(I) = \sqrt{(\sigma_\alpha^2 + \sigma_\beta^2)} + 0.3 * \sqrt{(\mu_\alpha^2 + \mu_\beta^2)} \quad (8)$$

Where in the above equations σ_α and σ_β are the standard deviations α and β, respectively, which are similarly their average, μ_α and μ_β.
Equation 9: Color enhancement factor (CEF) (Susstrunk and Winkler, 2003).

$$CEF = \frac{colorfu\ ln\ ess(CM)\ of\ output\ image}{colorfu\ ln\ ess\ (CM)\ of\ input\ image} \quad (9)$$

This criterion is used to distinguish the original (reduced) image from the enhanced image.

2.3 Construction and evaluation of a three-dimensional model

After applying the proposed contrast enhancement method to the images, it is necessary to perform aerial triangulation and calculate the camera's interior orientation parameters after generating a sparse point cloud. The constructed model is evaluated in this stage by selecting a set of points as a control point and another set as a check point. The check points are used to compare the accuracy of models generated in vertical and horizontal modes.
We calculated the error using relations (10) and (11) by comparing the difference between the horizontal coordinates of the check points and the three-dimensional points produced by the model via the two-dimensional Euclidean distance, as well as the difference between the vertical coordinates of the model points and the height of the check points (17).

$$E_{Pl} = \sqrt{(x_m - x_{ch})^2 + (y_m - y_{ch})^2} \quad (10)$$

$$E_{Al} = abs(z_m - z_{ch}) \quad (11)$$

Where x_m, y_m, and z_m represent the three-dimensional coordinates of the model's points, x_{ch}, y_{ch}, and z_{ch} represent the three-dimensional coordinates of the check points, and E_{Pl} and E_{Al} represent the horizontal and vertical errors, respectively. Additionally, various photogrammetric outputs are analyzed and evaluated by constructing and comparing quantitatively and qualitatively the digital elevation model and orthophoto mosaic to modes with contrast reduction.

3. EXPERIMENTAL RESULTS AND DISCUSSION

To evaluate the effect of the proposed algorithm, images taken by multi-rotor drones in various parts of Iran (Figure 2.) were evaluated. These images were taken at altitudes of 60 m and 90 m in the northwest of Qazvin at latitude 36.2337 and longitude 49.5118. We also took images at altitudes of 20 m and 40 m in the southern area of Sakineh Paradise in Karaj city at latitude 35.5322 and longitude 50.5244 (Fakhri et al., 2021). Moreover, we took images at altitudes of 80 m with latitude 35.1336 and longitude 46.4877 in the city of Helwan.

A. Northwest of Qazvin city B. South area of Sakineh Paradise in Karaj city C. City of Helwan

Figure 2. Study areas.

Additionally, images were captured using DJI's Phantom 4 Pro UAV (Figure 3.). As stated in Table 1, this UAV is controlled by a controller and equipped with a non-metric camera (Fakhri et al., 2021).

Figure 3. Phantom 4 Pro UAV.

Camera specifications	Phantom 4 Pro
Focal length	8.8 mm
FOV	70.0 Degree
Image Size	5472×3648
Sensor size	13.2×8.8 mm

Table 1. Specifications for drone cameras.

To begin with data analysis, a 3D model of low contrast images must be constructed. Thus, considering the high contrast of the images of the Qazvin and Karaj regions, a contrast reduction method was applied. Ultimately, using Halvan data with low image contrast, a 3D model was constructed. A 3D model was constructed using the proposed contrast-enhancement algorithm on the aforementioned images in the second stage. Figure 4 illustrates a sample of low-contrast, original and improved images are taken from a height of 90 m, together with their histogram.

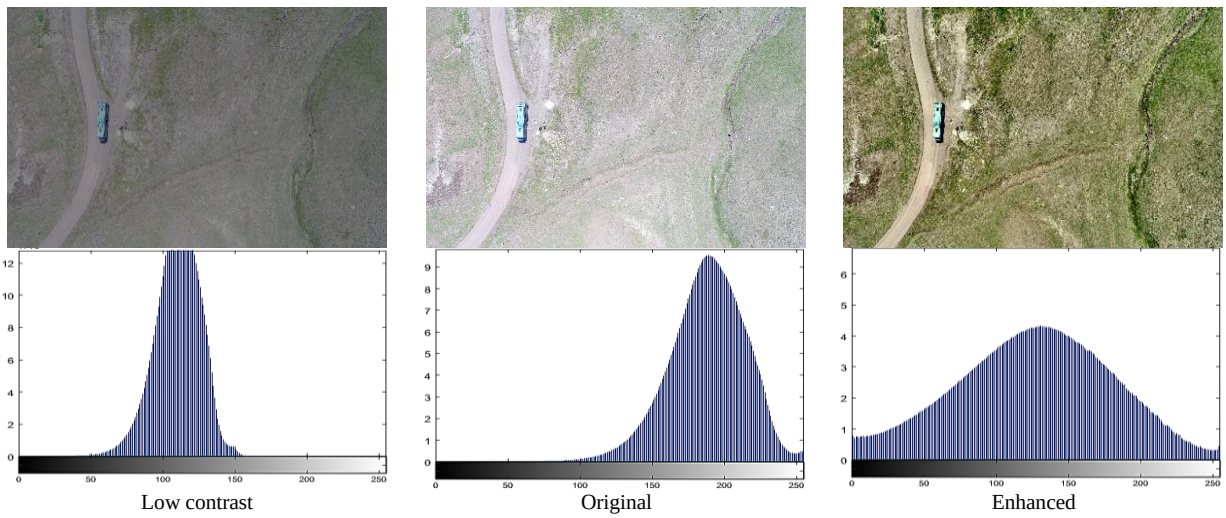

Low contrast Original Enhanced

Figure 4. A histogram and images with reduced contrast and enhanced.

As illustrated in the Figure 4, the proposed algorithm enhances the image histogram and enhances the contrast of the images. Triangulation and the construction of a 3D model were performed using Agisoft Metashape v1.5.5 software offered by Agisoft LLC. Additionally, the Python 3.10.1 programming language was utilized to implement the proposed algorithm and reduce the contrast of reference images.

3.1.1 Evaluation of results

The evaluation and interpretation of the obtained results are divided into two stages. The first section compares the proposed method for enhancing the contrast of images to current methods using assessment criteria. The second portion will analyse and assess the effect of enhancing the contrast of images on the accuracy of three-dimensional modelling when compared to the low contrast mode.

3.1.2 Evaluating the performance of a method for enhancing the contrast of images

To assess the performance of the image contrast improvement method in the first stage, the effect of the proposed method is compared to that of the original and reduced modes using a variety of evaluation criteria (Table 2).

Dataset		E	SD	PNSR	AMBE	γ	CM	CEF
Sakineh Paradise	Original	5.6998	25.8475	-	-	0.7237	10.1122	-
	Reduced	5.0099	13.8547	10.1139	53.1455	0.7185	6.0003	0.6221
	Enhanced	7.9256	76.9027	20.4598	12.1186	0.3901	26.3608	3.7709
Qazvin	Original	5.6245	22.314			0.7155	10.3145	-
	Reduced	5.0147	14.1731	10.2792	49.3874	0.7273	7.0993	0.5857
	Enhanced	7.9332	76.9040	20.4668	12.2148	0.3946	26.3710	3.7643
Helwan	Original	5.5321	27.145	-	-	0.7321	11.3189	-
	Reduced	-	-	-	-	-	-	-
	Enhanced	7.9358	76.9215	20.4514	12.1511	0.4001	26.1151	3.6778

As demonstrated in the Table 2, applying the proposed method to improve the contrast of images on the data set used resulted in a significant improvement in image quality when compared to the reduced and original modes. As a result, the proposed method will be evaluated and compared to several existing methods in the following step. 50 frames from various data sets will be chosen for this purpose, and the results will be presented in Table 3.

Methods	E	SD	PNSR	AMBE	γ	CM	CEF
HE	5.7591	73.6543	12.0922	16.4611	0.4063	–	–
CLAHE	6.9114	29.3949	22.3057	13.0904	0.6631	–	–
AMCE	7.9599	75.2166	12.0413	12.0873	0.3921	11.4620	1.6411
Proposed method	7.9358	76.9011	20.4663	12.1138	0.3911	26.3610	3.7743

Table 3. Comparison of the proposed method's performance to that of other commonly used contrast enhancement methods.

Based on the evaluations contained in Table 3, the following conclusions are drawn:

- *Entropy criterion*: Because the criterion above quantifies the content of image information and indicates the degree of uncertainty or unpredictability associated with the information included in an image, the more image information present, the higher the numerical value of the output and the greater its quality. The proposed approach and AMCE have demonstrated superior performance to alternative methods.
- *Standard Deviation Criterion*: Given that the criterion above quantifies the image information if the numerical value of the criterion above is greater in the enhanced image than in the low contrast image, the contrast enhancement algorithm performed better. Due to the image's low contrast of 14.1731, the proposed approaches of HE and AMCE enhanced the image's contrast.
- *Peak Signal-to-Noise Ratio Criterion*: Due to the fact that the preceding criterion checks an image's signal-to-noise ratio, the lower the image noise, the higher the result of this criterion. As a result, the proposed method and CLAHE result in the least amount of distortion in enhanced images.
- *Absolute Mean Brightness Error Criterion*: Because the aforementioned criterion quantifies the average brightness of the processed image, a low numerical value indicates that the image's average brightness is preserved. As a result, the proposed method and AMCE perform the best.
- *Linear Blur Index Criterion*: This criterion (γ) is used to evaluate the performance of contrast enhancement images, with a lower numerical output value indicating a higher performance of the contrast enhancement algorithm. According to the proposed method, AMCE and HE exhibit the best opacity.
- *Colorfulness Criterion*: As noted previously, CM and CEF criteria are only applicable to color images (RGB); thus, they cannot be employed in the HE and CLAHE approaches, which utilize images in the form of a grayscale band. This metric quantifies the quantity of color in an image, with a bigger numerical output value indicating more color detail. As a result, the proposed method is the most efficient.
- *Color Enhancement Factor Coefficient*: This criterion is a spectral component related to color saturation change; the higher the output's numerical value, the better. As a result, the proposed method is the most efficient.

In general, it is impossible to say which of the other methods presented performs better in all evaluation criteria, but the proposed method performs well in the majority of them; thus, it can be concluded that the proposed method provides more detail than UAV-based images and also better preserves the image's brightness.

3.1.3 Evaluating the effect of enhancing image contrast on the accuracy of modeling

Target targets were selected to assess the modeling's accuracy and their 3D coordinates measured prior to imaging operations in the research locations. As a result, 50% of the points primarily positioned in the project's corners were designated as check points. It should be noted that Agisoft Metashape software was used to generate a sparse point cloud and perform other steps associated with the construction of a 3D model. Images taken at 20 m, 40 m, 60 m, 80 m, and 90 m were used to generate the sparse point cloud and perform other steps associated with the construction of a 3D model. Thus, to generate a sparse point cloud, software-changeable parameters, in this case, the maximum tie and key points, as well as a search for key points, were done pixel by pixel. Figure 5 illustrates a sparse point cloud generated by the software in both low-contrast and enhanced modes from heights of 80 and 90 m.

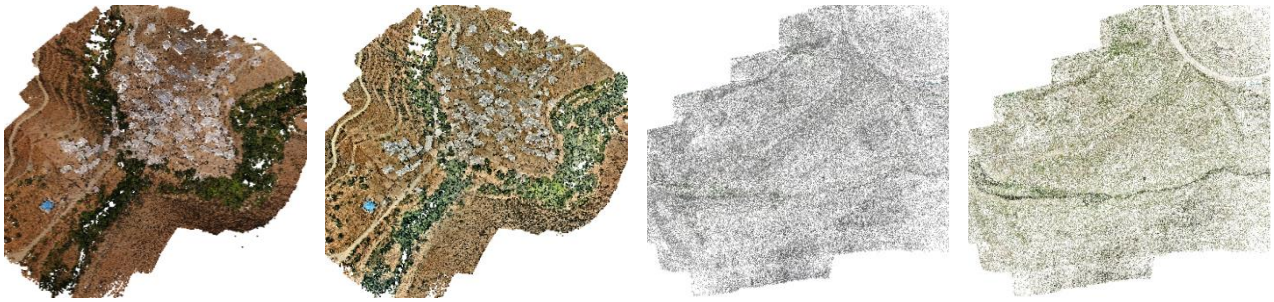

A. Images with a low contrast Point cloud produced from Helwan area at an altitude of 80 m
B. Images with enhanced contrast
C. Images with reduced contrast Point cloud produced from Qazvin area at an altitude of 90 m
D. Images with enhanced contrast

Figure 5. A sparse point cloud obtained at an altitude of 80 and 90 m.

By comparing the density of tie and key points extracted from low contrast and enhanced contrast images, it was discovered that the density of points in the enhanced contrast images is greater than the density of points in the low contrast images. Figure 6 illustrates how the algorithms extracted the tie and key points from a contrast-enhanced image taken at an altitude of 90 m.

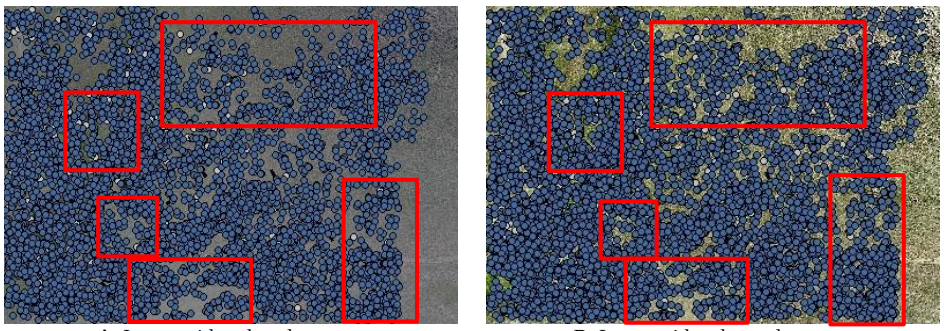

A. Image with reduced contrast
B. Image with enhanced contrast

Figure 6. An illustration of the tie points extracted from a 90-meter-altitude image.

When utilizing contrast-enhanced images, as seen in the red boxes above, the density and increase of tie points are greater than when using low-contrast images. As a result, a comparison was made based on determining the number of tie points and the amount of reprojection error in each of the models produced in the above two cases, and it was discovered that after contrast enhancement and the average reprojection error, tie points in each model increased by about 6 to 10%. It has decreased by approximately 8% to 11%. Figure 7 depicts the number of tie points and reprojection error in models with five distinct flying altitudes in two modes with low contrast images and contrast enhancement. The number of tie points and the horizontal axis show the types of models generated in the vertical axis A diagram, and the amount of reprojection error and the horizontal axis indicate the types of models produced in the vertical axis B diagram.

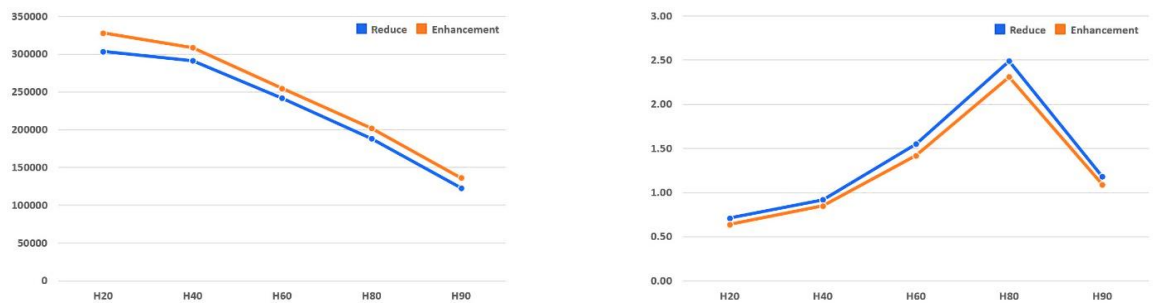

A. The number of tie points diagram
B. Reprojection error diagram

Figure 7. At different flying altitudes and in low contrast and enhanced modes, the number of tie points and reprojection error is shown in a diagram.

There is an increase of around 10% in the number of tie points and a reprojection of about 10% in all models built from contrast-enhanced images (orange axis) compared to models made from lower contrast images (blue axis) as can be seen in the graphs above. Control points and check points were also added to the generated points cloud in order to study the effect of increasing image contrast on modelling accuracy. Calculations will be made. Figure 8 depicts the horizontal and vertical error acquired on the check points at five different flight altitudes and two low contrast modes and contrast enhancement. The horizontal axis and the error values of the check points indicate the types of models produced in the two ways of utilizing low-contrast images and enhancing contrast in the vertical sub-axis diagram.

A. The amount of vertical error B. The amount of horizontal error

Figure 8. Diagram depicting the amount of error obtained on the check points at five different flight altitudes and two modes (low contrast and enhanced contrast).

According to the schematics above, image enhancement contrast has no significant effect on the accuracy of check points in the horizontal and vertical directions. Other photogrammetry products were also produced to examine the effect of enhancing image contrast on the DEM and orthophoto mosaic. At 80 m and 90 m, Figure 9 illustrates an example of a DEM and orthophoto mosaic.

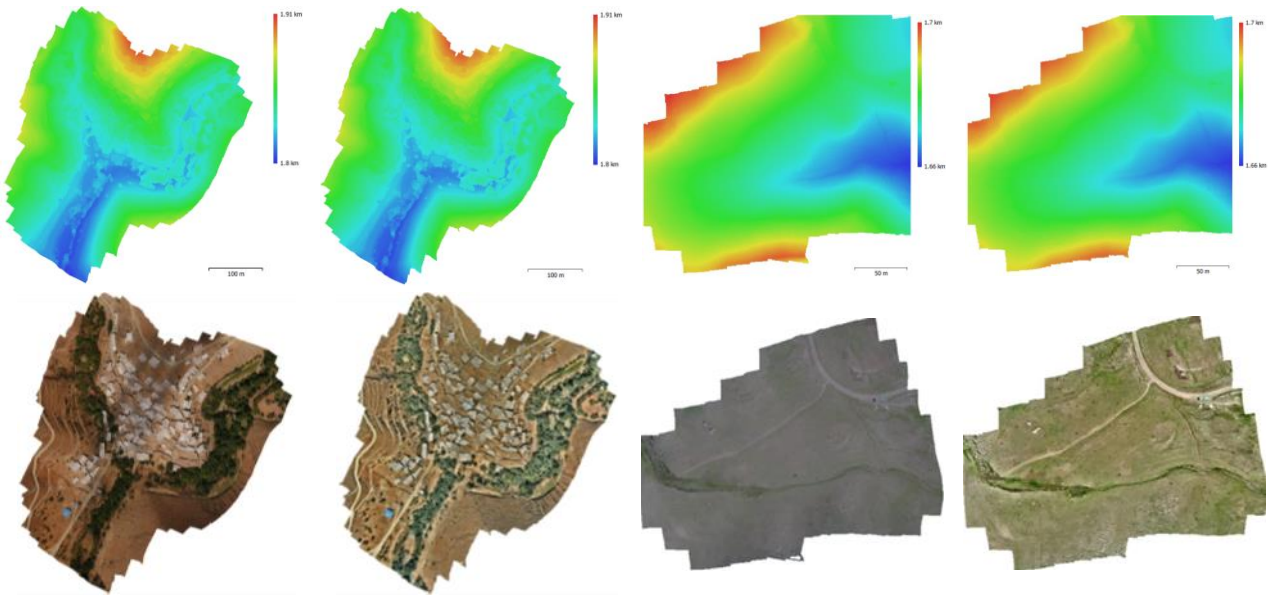

A. Low contrast images B. Contrast enhancement images C. Contrast reduction images D. Contrast enhancement images
DEM and orthophoto mosaic 80 m DEM and orthophoto mosaic 90 m

Figure 9. A DEM and orthophoto mosaic generated at the height of 90 meters.

The orthophoto mosaic generated by the enhanced images has a better texture than the lower contrast mode, as shown in the Figure 9, which can improve the cartograph's accuracy in sketching numerous features in more detail. On two samples of Halvan images, the effect of enhancing image contrast on increasing the quality and accuracy of the orthophoto mosaic produced to execute the feature drawings is demonstrated in Figure 10.

A. Enhanced contrast images B. Low contrast images

Figure10. Two examples of the effect of enhancing image contrast on the quality and accuracy of orthophoto mosaic produced from an altitude of 80 meters.

Drawing features on orthophoto mosaic generated from contrast-enhanced images can be done with more precision and detail, as shown in the Figure 10. The outputs related to the evaluations completed in this research are displayed in Table 4 on three study areas from five different flying altitudes.

Dataset	Reprojection error (px)		Tie points		Check points RMSE(m) XY		Z		DEM resolution (cm/px)	
	Reduce	Enh.	Reduce	Enh.	Reduce	Enh.	Red.	Enh.	Reduce	Enh.
H 20	0.71	0.64	303,709	328,006	0.018	0.017	0.023	0.023	1.35	1.23
H 40	0.92	0.85	291,301	308,780	0.021	0.021	0.020	0.019	6.95	6.47
H 60	1.55	1.42	242,007	254,768	0.035	0.034	0.041	0.041	32.7	30.1
H 80	2.49	2.31	188,242	202,021	0.072	0.072	0.071	0.070	39.5	38.2
H 90	1.18	1.09	122,918	136,322	0.029	0.029	0.024	0.023	61.3	58.4

Table 4. The results of UAV products for different dataset.

The number of tie points in all models produced using images with enhanced contrast is approximately 10% higher than the low contrast mode, and the reprojection error is reduced by around 10%, as shown in Table 4. In the generated of DTM models, there is also resolution enhancement approximately 2cm/pixel. Of course, the amount of horizontal and vertical error between.

4. CONCLUSION

Due to the variety of applications for UAV photogrammetry, such as mapping and the construction of three-dimensional models, we are occasionally required to acquire images in low-light settings. Due to the scope of UAV-assisted projects, these conditions may not be applicable to the entire region.

As a result of the shadow, one section of the object will receive more light while another will receive less. This disturbs the point cloud generation process and results in an inadequate texture for the overall model produced. As a result, the influence of contrast enhancement on images in dark and low contrast areas has been investigated in this article. Because many techniques are offered in histogram equalization methods in order to increase the grayscale range of the image.

To illustrate the proposed algorithm, the conventional contrast-enhancement algorithms with the greatest performance on various images were used in this research. However, multiple error criteria were used to illustrate the proposed method's performance to show that the new algorithm provided significantly higher accuracy. Thus, by applying the proposed technique to low contrast images from three different study locations and five different flight altitudes, photogrammetric products such as dense and sparse point clouds, digital elevation models, and orthophoto mosaic were generated in both cases.

The results indicated that the number of tie points extracted after using the proposed contrast-enhancement technique to low-contrast images increased by approximately 10%, increasing the density of the point cloud. Contrast enhancement of the images also results in a relative gain of approximately 2 cm/px in the resolution of the digital elevation model. Additionally, reprojection error was reduced by approximately 10%, although calibration parameters and check point error did not differ significantly between images with low contrast and images enhanced by the algorithm.

REFERENCES

A. Ballabeni, F.I. Apollonio, M. Gaiani, F. Remondino, 2015. Advances in Image Pre-processing to Improve Automated 3D Reconstruction, International Archives of the Photogrammetry, Remote Sensing and Spatial Information Sciences.

A. Hore, D. Ziou, 2010. Image quality metrics: PSNR vs. SSIM, in: 2010 20th international conference on pattern recognition, IEEE, pp. 2366-2369.

A. Kaufmann, 1975. Introduction to the theory of fuzzy subsets, Academic press.

C. E. Shannon, 1948. A mathematical theory of communication. The Bell System Technical Journal, 27, 379-423.

C. Tomasi, R. Manduchi, 1998. Bilateral filtering for gray and color images, in: Sixth International Conference on Computer Vision (IEEE Cat. No.98CH36271), pp. 839-846.

C. Wu, 2013. Towards linear-time incremental structure from motion, in: 3D Vision-3DV 2013, 2013 International Conference on, IEEE, pp. 127-134.

D. Skarlatos, S. Kiparissi, 2012. Comparison of laser scanning, photogrammetry and SFM-MVS pipeline applied in structures and artificial surfaces.

E. Demetrescu, E. d'Annibale, D. Ferdani, B. Fanini, 2020. Digital replica of cultural landscapes: An experimental reality-based workflow to create realistic, interactive open world experiences, Journal of Cultural Heritage, 41, 125-141.

F. Bellavia, M. Fanfani, C. Colombo, 2015. Fast Adaptive Frame Preprocessing for 3D Reconstruction, in: VISAPP (3), pp. 260-267.

G. Verhoeven, W. Karel, S. Štuhec, M. Doneus, I. Trinks, N. Pfeifer, 2015. Mind your grey tones: examining the influence of decolourization methods on interest point extraction and matching for architectural image-based modelling, in: 3D-Arch 2015: 3D Virtual Reconstruction and Visualization of Complex Architectures, Copernicus Gesellschaft, pp. 307-314.

H. Yao, R. Qin, X. Chen, 2019. Unmanned Aerial Vehicle for Remote Sensing Applications—A Review, Remote Sensing, 11(12).

I. Recommendation, 2005. 1700, Characteristics of Composite Video Signals for Conventional Analogue Television Systems, International Telecommunication Union, Geneva, Switzerland.

J. C. M. Román, H. Legal-Ayala, J.L.V. Noguera, 2017. Top-hat transform for enhancement of aerial thermal images, in: 2017 30th SIBGRAPI Conference on Graphics, Patterns and Images (SIBGRAPI), IEEE, pp. 277-284.

J. Hertz, A. Krogh, R.G. Palmer, 2018. Introduction to the theory of neural computation, CRC Press.

J. P. Arroyo-Mora, M. Kalacska, T. Løke, D. Schläpfer, N.C. Coops, O. Lucanus, G. Leblanc, 2021. Assessing the impact of illumination on UAV pushbroom hyperspectral imagery collected under various cloud cover conditions, Remote Sensing of Environment, 258, 112396.

J. Revuelto, J.I. López-Moreno, E. Alonso-González, 2021. Light and shadow in mapping alpine snowpack with unmanned aerial vehicles in the absence of ground control points, Water Resources Research, 57(6), e2020WR028980.

K. J. Chang, C.-W. Tseng, C.-M. Tseng, T.-C. Liao, C.-J. Yang, 2020. Application of unmanned aerial vehicle (uav)-acquired topography for quantifying typhoon-driven landslide volume and its potential topographic impact on rivers in mountainous catchments, Applied Sciences, 10(17), 6102.

K. Jacq, E. Ployon, W. Rapuc, C. Blanchet, C. Pignol, D. Coquin, B. Fanget, 2021. Structure-from-motion, multi-view stereo photogrammetry applied to line-scan sediment core images, Journal of Paleolimnology, 1-12.

K. Zuiderveld, 1994. Contrast limited adaptive histogram equalization, Graphics gems, 474-485.

M. Dymczyk, E. Stumm, J. Nieto, R. Siegwart, I. Gilitschenski, 2016. Will it last? learning stable features for long-term visual localization, in: 3D Vision (3DV), 2016 Fourth International Conference on, IEEE, pp. 572-581.

M. Godinho, R. Machete, M. Ponte, A.P. Falcão, A.B. Gonçalves, R. Bento, 2020. BIM as a resource in heritage management: An application for the National Palace of Sintra, Portugal, Journal of Cultural Heritage, 43, 153-162.

M. Gaiani, F. Remondino, F.I. Apollonio, A. Ballabeni, 2016. An advanced pre-processing pipeline to improve automated photogrammetric reconstructions of architectural scenes, Remote sensing, 8(3),178.

M. Jarzabek-Rychard, M. Karpina, 2016. QUALITY ANALYSIS ON 3D BUIDLING MODELS RECONSTRUCTED FROM UAV IMAGERY, International Archives of the Photogrammetry, Remote Sensing and Spatial Information Sciences, 41.

M. Lv, D. Tu, X. Tang, Y. Liu, S. Shen, 2021. Semantically Guided Multi-View Stereo for Dense 3D Road Mapping, in: 2021 IEEE International Conference on Robotics and Automation (ICRA), pp. 11189-11195.

M. Pepe, D. Costantino, Techniques, tools, 2020. platforms and algorithms in close range photogrammetry in building 3D model and 2D representation of objects and complex architectures, Comput. Aided Des. Appl, 18, 42-65.

N. Phanthuna, 2015. Contrast image enhancement using multi-histogram equalization, International Journal of Advanced Culture Technology, 3(2), 161-170.

R. Maini, H. Aggarwal, 2010. A comprehensive review of image enhancement techniques, arXiv preprint arXiv:1003.4053.

R. Qin, A. Gruen, 2021. The role of machine intelligence in photogrammetric 3D modeling – an overview and perspectives, International Journal of Digital Earth, 14(1), 15-31.

S. A. Alasal, M. Alsmirat, Q.B. Baker, Y. Jararweh, 2018. Improving Passive 3D Model Reconstruction using Image Enhancement, in: 2018 6th International Conference on Multimedia Computing and Systems (ICMCS), IEEE, pp. 1-7.

S. A. Fakhri, H. Latifi, 2021. A Consumer Grade UAV-Based Framework to Estimate Structural Attributes of Coppice and High Oak Forest Stands in Semi-Arid Regions, Remote Sensing, 13(21), 4367.

S. A. Fakhri, M. Saadatseresht, M. Varshosaz, H. ZAKERI, 2021. Evaluation of UAV Photogrammetric capability in Road Pavement Cracks Detection, Amirkabir Journal of Civil Engineering.

S. A. Fakhri, S. A Fakhri, 2019. Investigating the Effect of Pso Algorithm on Reducing Control Points in Camera Calibration, ISPRS-International Archives of the

Photogrammetry, Remote Sensing and Spatial Information Sciences, 4218, 363-369.

S. E. Susstrunk, S. Winkler, 2003. Color image quality on the internet, in: Internet imaging V, International Society for Optics and Photonics, pp. 118-131.

S. Lal, A. Narasimhadhan, R. Kumar, 2015. Automatic method for contrast enhancement of natural color images, Journal of Electrical Engineering and Technology, 10(3), 1233-1243.

S. M. Pizer, E.P. Amburn, J.D. Austin, R. Cromartie, A. Geselowitz, T. Greer, B. ter Haar Romeny, J.B. Zimmerman, K. Zuiderveld, 1987. Adaptive histogram equalization and its variations, Computer vision, graphics, and image processing, 39(3), 355-368.

S. Paris, P. Kornprobst, J. Tumblin, F. Durand, 2009. Bilateral filtering: Theory and applications, Now Publishers Inc.

S. Standard, 2003. System M/NTSC Composite Video Signals, Bit-Parallel Digital Interface.

T. Lestari, A. Luthfi, 2019. Retinal Blood Vessel Segmentation using Gaussian Filter, in: Journal of Physics: Conference Series, IOP Publishing, pp. 012023.

T. Luhmann, M. Chizhova, D. Gorkovchuk, 2020. Fusion of UAV and Terrestrial Photogrammetry with Laser Scanning for 3D Reconstruction of Historic Churches in Georgia, Drones, 4(3), 53.

T. Moons, L. Van Gool, M. Vergauwe, 2009. 3D reconstruction from multiple images: principles, Now Publishers Inc.

W. Hartmann, M. Havlena, K. Schindler, 2014. Predicting matchability, in: Proceedings of the IEEE Conference on Computer Vision and Pattern Recognition, pp. 9-16.